# Coastal flooding will disproportionately impact people on river deltas

Douglas A. Edmonds[1*], Rebecca L. Caldwell[1,2], Eduardo Brondizio[3], and Sacha Siani[3]

(1) Department of Earth and Atmospheric Sciences, Indiana University
(2) Now at Chevron Energy Technology Company, Chevron Corporation, Houston, TX 77002, USA
(3) Department of Anthropology, Indiana University

*to whom correspondence should be addressed: edmondsd@indiana.edu

## Introductory Paragraph

Climate change is intensifying tropical cyclones[1], accelerating sea-level rise[2], and increasing coastal flooding[3]. Coastal flooding will not affect all environments equally, and river deltas are especially vulnerable because of their low elevations[4], densely populated cities[5-7], and river channels that propagate coastal floods inland[8]. Yet, we do not know how many people live on deltas and their exposure to flooding. Using a new global dataset of 2,174 river delta locations[9] and areas, we show that in 2017 there were 339 million people living on river deltas with 329 million (or 97%) living in developing and least-developed economies. We show that geographically, 88% of people on river deltas live in the same zone as most tropical cyclone activity[3]. Of all the people exposed to tropical cyclone flooding[10], our analysis suggests 41% (or 31 million) live on deltas. Of these, 92% (or 28 million) live in developing or least developed economies, where lacking infrastructure for hazard mitigation increases their vulnerability. Furthermore, 80% (or 25 million) live on sediment-starved deltas that are unable to naturally mitigate flooding through sediment deposition. The 2019 IPCC special report makes it clear that coastal flooding will increase[11], and it is essential that we reframe the concept of coastal flooding as a problem that will disproportionately impact people on river deltas, particularly in developing and least-developed countries.

## Main Text

People have been exploiting the resources and natural infrastructure of river deltas for at least 7,000 years[12]. Most civilizations preferentially grew around coastlines and river deltas because the abundant food resources provided by the sea, the fertile soils, and their positions as transportation hubs fueled development of urban economies and lifestyles[7,13,14]. This has scarcely changed today as the most densely populated cities in the world are on low-lying deltaic landforms[15,16].

The presence of people on river deltas for millennia and the modification of watersheds have had adverse effects on deltaic landforms[17]. To accommodate the burgeoning populations, humans engineered rivers[18], withdrew subsurface resources[19], and changed the landcover. These changes reduced river sediment supply[20] and increased subsurface subsidence[21], which together initiated erosion and land loss in some major deltas[4,22,23]. Sinking land surfaces locally accelerates relative sea-level change[24] and deltaic areas at risk of coastal flooding could grow by 50% under current scenarios for sea-level rise[4]. Exacerbating these concerns, hydrological extremes, such as tropical cyclones[3], are also projected to become more intense[1]. To plan for and mitigate these hazards, we need to know how many people live on deltas in different socioeconomic contexts around the planet, and their vulnerability to flood hazards.

Living on river deltas is also challenging because multiple socioeconomic stressors intersect, which increases vulnerability to hazards, like flooding. Most deltaic populations are in urban areas of developing and least-developed economies, or in high-density rural areas, such as in the Ganges-Brahmaputra and Mekong deltas[25]. In these areas, low-income residents often occupy low-lying areas prone to storm surge flooding. These areas also have high levels of infrastructure deficiencies, such as inadequate or nonexistent storm and surface drainage, piped water, collection of domestic effluent and trash, paved roads and/or accessible pathways, and the inhabitants are experiencing water pollution, poor and subnormal housing infrastructure, and limited access to public services[26]. These stressors undermine both the generic (infrastructural) and specific (individual and group) adaptive capacities of deltaic populations to flood hazards[27,28].

## Defining the global population on river deltas

Estimates of the number of people living on deltas vary widely[5,6,29] because there is no widely agreed upon definition of deltaic area and thus there have been few attempts to survey the global deltaic population. Defining delta area is challenging because river deltas are depositional sedimentary bodies that rarely have a fixed mappable boundary that defines delta extent. To address these challenges, we developed a new global dataset of delta area to define the global deltaic population, and its vulnerability to flood hazards. We define delta area as the extent of geomorphic activity created by deltaic channel movement, and delta progradation. We focus on activity because it encompasses the channel network, which creates the resources and natural infrastructures that make deltas attractive sites for habitation, and defines the most the most flood-prone zone and most probable area of active deposition.

We measure deltaic area by defining five points that encompass deltaic activity. We mark visible traces of deltaic activity with two points capturing the lateral extent of deposition along the shoreline, and with three points enclosing the up and downstream extent of deposition (Extended Data Figures 1, 2; Supplementary Table 1). The convex hull around these five points defines a delta area polygon (Extended Data Figures 1c, 3). While these choices introduce some subjectivity, this method is consistent with previously measured deltaic areas (Extended Data Figure 4 and Table 2; see Methods). Within each delta polygon, we extract the topography from a 30 arc-second elevation model, and we define each pixel as deltaic if they meet an elevation criterion; non-deltaic pixels are removed (see Methods). The geomorphic area is the areal sum of all deltaic pixels within the polygon. The habitable area is the cumulative sum of all land minus all water, including channels, water bodies, and ocean. Water presence is defined at a subpixel level from global and country-level water masks[17]. Deltaic population is the cumulative populations of all deltaic pixels within each polygon. Population counts come from Oak Ridge National Laboratory's 30 arc-second LandScan data from years 2000, 2010, and 2017 (see Methods). We estimate the population vulnerable to flood hazards based on direct exposure to floods[10] (i.e., residing in the ocean-connected 100-year floodplain, see Methods). Our flood exposures do not account for flood protection.

The socioeconomic conditions associated with development categories defined by the 2019 UN World Economic Situation and Prospects.

**Global distribution of deltaic area and population**

Our results show that deltas occupy 0.57% of the earth's land surface area, but in 2017 they contained 4.5% of the global population (Figure 1). Globally, river deltas contain 847,936 $km^2$ of geomorphic area, 710,179 $km^2$ (or 84%) of which is habitable (see Methods) (Figure 1A). Roughly, 77% of geomorphic area is found between 10°S and 35°N (Figure 1C). The largest deltas are the Amazon and the Ganges-Brahmaputra, which contain 84,429, and 80,174 $km^2$ of geomorphic area, respectively (Extended Data Table 1).

In 2017, there were 339 million people living on river deltas. People generally do not inhabit deltas at high and low latitudes, and instead 88% of all people living on deltas are commonly found in a narrower zone from 10°N to 35°N (Figure 1C, D). The most populated delta is the Ganges-Brahmaputra with 105 million people, over half of which are in rural areas[25], and the second most populated is the Nile delta at 45 million (Extended Data Table 1). In fact, the ten most populated deltas account for 78% of the total population.

Deltas host some of the world's most densely populated cities. In our dataset, there are seven mega densely populated deltas with more than 10,000 people/$km^2$ (Extended Data Table 1). The Neva River delta in Russia, which contains St. Petersburg, is the most densely populated at 17,062 people/$km^2$. If all 339 million people were evenly distributed across all deltaic habitable area, there would be 478 people/$km^2$ living at a density 8 times the global average. If we consider the population per delta, larger deltas tend to host larger populations (Figure 2A) and the median population density is 34 people/$km^2$ and many deltas ($n$ = 478) have fewer than 1 person/$km^2$ (Figure 2B).

**Vulnerability of deltaic population to coastal flooding**

An astounding number of people on river deltas (88% or 298 million) live in the same latitudinal zone as tropical cyclone genesis in the Northern hemisphere[3] putting them in the path of major coastal storms. Whether not these people are vulnerable to coastal flooding depends on both physical and socioeconomic factors. From a physical standpoint, vulnerability to coastal flooding depends on where people live relative to sea-level for a given storm surge height. People are spread out evenly over deltaic elevations; roughly 50% of both deltaic area and population are below or above an elevation of 6.5 m (Figure 2C). The lowest elevation areas are more vulnerable, and 9.4% of deltaic area and 5.9% of people (or 18 million people in 2017) are at or below 1 m elevation (Figure 2C). Cross-referencing our data with recent global estimates of the 100-yr storm surge elevation[10], we find that 11% of habitable deltaic area and 9.1% of all people living on deltas are in the 100-yr storm surge floodplain (see Methods). Across the globe, 76 million people are exposed to a 100-year storm surge flood[10], and nearly 41% of those people (or 31 million people in 2017) live in river deltas.

Socioeconomic factors also influence vulnerability because they correlate with the quality of physical infrastructure and access to social services, and thus, the ability of deltaic populations to respond to flood risk. Previous global analysis[26] indicated that urban areas in developing and under-developed countries have statistically significant lower socioeconomic (e.g., literacy rate, mortality, employment, poverty rate, and quality of life index) and infrastructure (e.g., improved water, percentage slum households, internet access, and city prosperity index) conditions compared to developed countries, both of which directly affect local vulnerability to flooding. Such deficiencies are equally or even more pronounced in high-density rural areas, such as among the large deltaic populations of the Ganges-Brahamaputra and the Mekong[25]. This is problematic because in 2017, deltas in developing and least-developed countries accounted for 61% (or 207 million people) and 36% (or 121 million people) of the total deltaic population, respectively. These populations are also growing faster than those in developed countries. Between 2000 and 2017, the global population on river deltas grew by 34% (86 million people), virtually all of it in developing and least-developed countries (Figure 3). Of the people living in the 100-year floodplain, 92% are in deltas in developing and least-developed countries (Figure 3).

Regions of vulnerable deltaic populations are not evenly distributed globally. In 2017, for instance, 76% of the total population living in deltas were in the Asia-Pacific regions (259 million people), followed by 18% in Africa (62 million people), 2.8% in the Americas (9.5 million people), and 1.1% in Europe and Central Asia (3.8 million people) (Figure 1C). Of the deltaic population that lives within the 100-year floodplain, the majority are in the Asia-Pacific region (25 million people), followed by also large populations the Europe-Central Asia (3.8 million people), Africa (3.3 million people), and to a lesser extent, the Americas (~0.5 million people) (Extended Data Figure 5).

## **Mitigating coastal flooding**

In response to this vulnerability, many deltaic communities will likely consider adaptation and mitigation measures. Some communities have already adopted engineering solutions to mitigate hazards (e.g., the Mississippi, Rhine, Mekong, and Nile) because of the significant flooding risk[4,17]. But, engineering solutions are expensive and can fail when floods exceed the design limitations. A more natural solution to limit coastal flooding is for deltaic growth to fill in these flood zones with sediment[30]. Indeed, this is what a delta does as it grows; areas that are repeatedly flooded receive more sediment[31]. In this way, deltas can self-regulate flooding if the volume between the land surface and the 100-yr storm surge elevation can be filled by sediment supplied from the river. But most deltas are at the mouths of the world's major rivers[9], and they are sediment starved because of dam construction upstream[4,20]. In fact, deltas with large floodplain areas (>100 km$^2$) are sediment starved and will not be able to naturally aggrade these flood zones (Figure 4). In 2017, 80% (or 25 million) of people living in the world's deltaic 100-year floodplains were on sediment-starved deltas. Flood mitigation measures on sediment starved deltas will increasingly have to rely on hard engineering solutions because these larger deltas can no longer naturally aggrade their floodplain surfaces. By contrast, smaller deltas still can naturally aggrade their surface, something noted by Giosan et al.[30] (Figure 4).

In sum, our analysis shows that if coastal flooding intensifies, as predicted[11], it will disproportionately impact people on river deltas, the vast majority of which are living on sediment starved deltas in developing and least-developed countries. The population estimates we present here are likely a minimum because global storm surge models[10] currently do not account for compound events created by the interaction of storm surge, rivers, and tides[32,33], changes in relative sea-level, and inaccuracies in elevation models at the coast[34]. Consider that if we add 1 m of sea level rise to the 100-yr storm surge elevation, the number of people vulnerable to flooding increases by 75% to 54 million. To more accurately assess risk and vulnerability we need better elevation and storm surge models for deltaic environments[35].

**Main Text Figures and Captions**

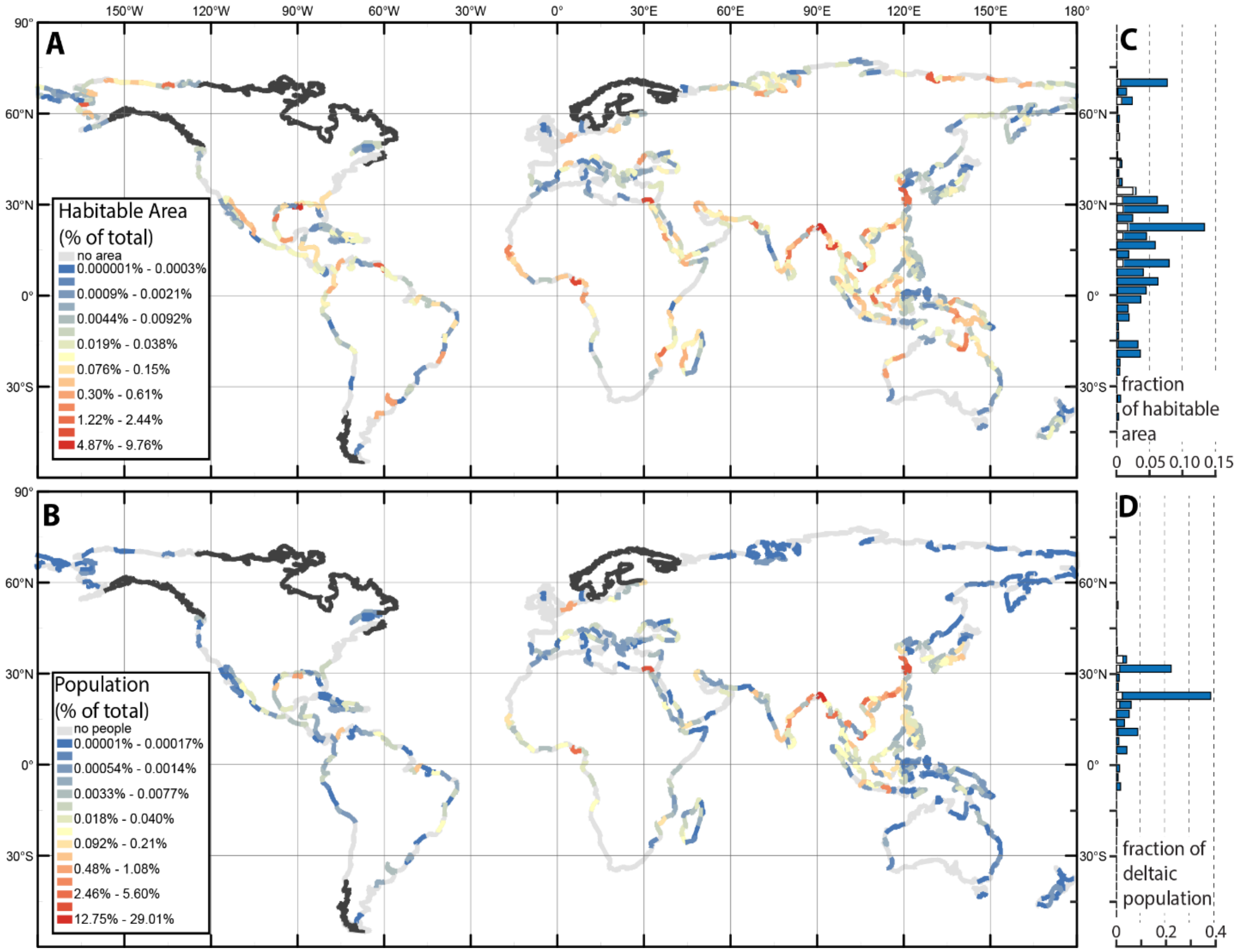


**Figure 1: Global distribution of deltaic area and population.** A, B) Total deltaic area and population per 3° lengths of coastline. Lengths of coastlines are colored by the percentage of area or population they contain relative to the entire dataset. Black lines correspond to shorelines that were unmapped in Caldwell et al.[9]. C, D) Histograms showing the latitudinal distribution (3° bins) of habitable area and population. White bars show the proportion of area and people in the 100-year storm surge floodplain.

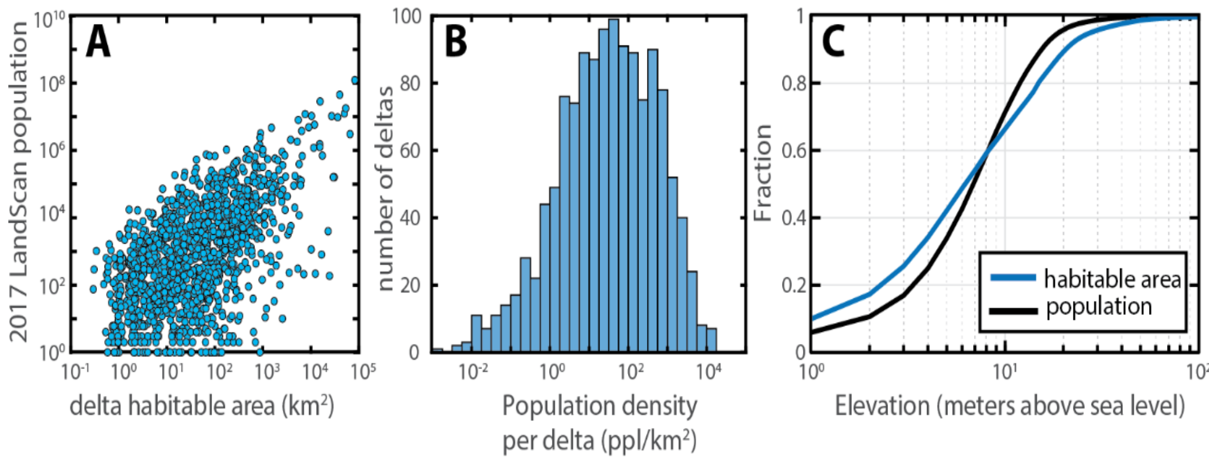


**Figure 2: Statistics of delta area and population.** A) Population scales with habitable area. Each dot represents a single delta ($n$ = 1,652). There are 522 deltas either with no measurable population or habitable area; B) Histogram of deltaic population density calculated as the total population for each delta relative to the habitable area (n = 1,652). C) Cumulative distribution function of habitable area and population as a function of elevation

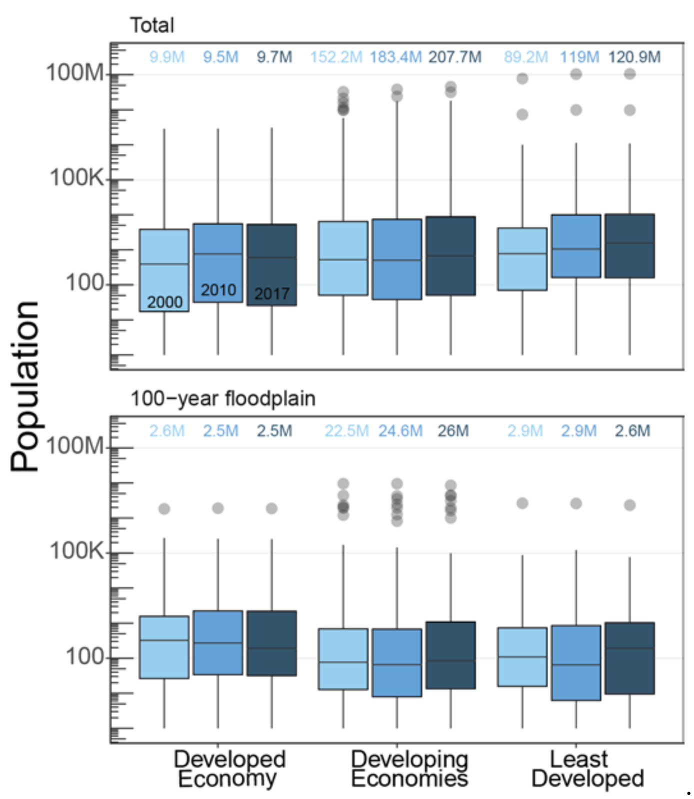


**Figure 3: Population distribution for deltas classified according to UN development categories for their respective countries.** The box and whisker plots show the distribution for all deltas with a given economic development category for each year. The median value is the horizonal line in the box, box width corresponds to the upper and lower quartiles. The whisker lengths represent the lower and upper 25% quartile distribution of all deltas within a category, and gray dots are outliers. Colored numbers refer to the total in each category

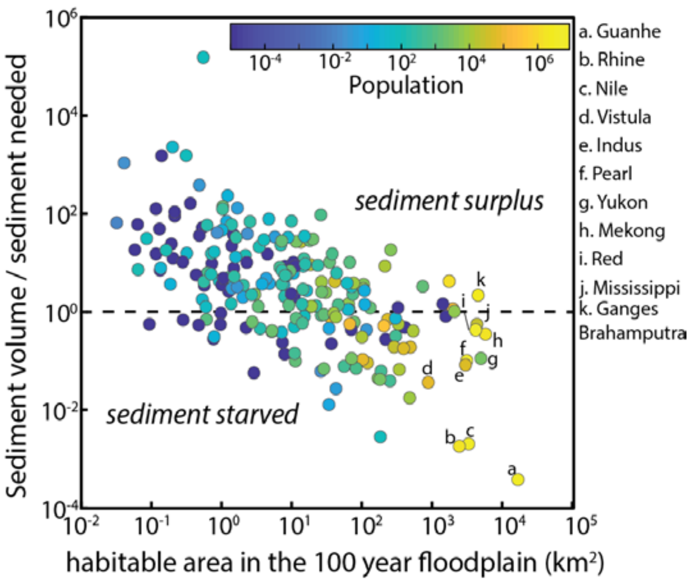


**Figure 4: Sediment starved deltas contain more area and people in the 100-year floodplain.** Sediment volume is the depositional volume created by 100 years of river sediment supply[36] with a porosity fraction of 0.4 and sediment retention fraction of 0.35 (ref. [37]). Sediment needed is the volume of space between the 100-yr storm surge elevation and the land surface elevation. Deltas with a value greater than one have a sediment surplus and may be able to aggrade their floodplain to the elevation of the 100-year storm surge, and those with value less than one are sediment starved. Each dot represents a delta that has a sediment discharge value (*n* = 287).

# ***Methods***

## **1. Delta Area Mapping**

We define a delta area for each delta identified in Caldwell et al.[9]. Defining delta area is not trivial. In fact, of the existing studies that report deltaic area[4-6,24,38-42], the method for defining delta area is not consistent and in many cases is not described. As an example, consider the Vistula delta in Poland. In two different studies[4,38] the size is listed as 500 $km^2$ and 1,490 $km^2$. The method for determining the area in either case is not clearly explained. These kinds of discrepancies probably arise because defining the size of any depositional sedimentary body, like river deltas, is difficult because the thickness of deposition usually exponentially declines away from the point source[43]. Tracing exponentially declining deposition to the absolute margin of the deposit can be difficult, if not impossible, because the thickness of sediment deposition becomes vanishingly small. If the thickness of the deposit is perfectly known then one could define a semi-arbitrary boundary for the deposit edge, such as the e-folding length. However, sediment thicknesses for the world's coastlines that distinguish deltaic and non-deltaic deposition are not easily obtainable and defining delta size based on deposit thickness is not feasible. Instead, the most reliable data that we can use to define delta area are from photographs. Even from photographs, the extent of delta deposition is difficult to measure because it may interfinger with adjacent coastal environments creating a gradual transition that is difficult to map on a photograph. Of course, in some cases this may not be true, because if deposition is confined, within a valley for example, then the contact between deltaic and nondeltaic area can be mapped with confidence (Extended Data Figure 3a,b). But not all deltas form in valleys or places where their lateral contacts are visible, so this criterion cannot be universally applied.

Considering these challenges, the method we use to define delta area relies only on surficial information and defines delta area as including all land where deltaic processes are visibly active currently or recently. We adopted a simplified approach using five points to define area because it can be applied to every delta and only requires a photograph to implement. The delta area is calculated as the convex hull contained by: the delta node (*DN*), two lateral shoreline extents (*S1* and *S2*), the main river mouth (RM), and the basinward-most extent towards the open marine basin (*OB*). Detailed definitions of these points are provided in section 4.

Our method captures the first-order shape of a delta with operational definitions that are straightforward to apply. Admittedly, this approximation does not perfectly capture all intricacies of deltaic shape (Extended Data Figure 3), but as we show later this method generates estimates consistent with previously published data. The drawback to our chosen approach is that it introduces subjectivity in selecting the points that make up the delta polygon. We provide all our point selections so that individual decisions can be assessed on a case-by-case basis (see supplementary table 1).

## **2. Considerations for locating delta extent points**

The locations of the five points that define delta area were chosen using the most recent imagery available in Google Earth. Due to the rapidly changing nature of deltaic land, some of these point locations could change with time, and may differ from the points we define at the time of this paper.

*River Mouth (RM)*

On each delta we marked the location of the widest river mouth in the distributary network. We measure channel width at the shoreline.

*Delta node (DN)*
The delta node is defined as either (1) the upstream-most bifurcation of the parent channel (Extended data Fig. 2a), or if no bifurcation is present as (2) the intersection of the main channel with the deltaic shoreline vector ($L_S$) which is defined as the line connecting *S1* and *S2* (Extended Data Figure 2b). In the case where (1) and (2) exists, the delta node that is furthest upstream is chosen as the *DN* location. If a delta does not have a distributary network, then option (2) is chosen as the delta node.

*Lateral shoreline extent points (S1 and S2)*

The lateral shoreline extent points are defined as either (1) the locations on the shoreline that mark the boundary between deltaic protrusion and the regional non-deltaic shoreline (Extended Data Figure 3c), or (2) the lateral-most extent of channel activity, defined by an active or inactive channel (Extended Data Figure 1a). If both (1) and (2) exist, the lateral shoreline extent locations that are farthest laterally from the center of the delta sets the *S1* and *S2* locations. Point *S1* is on the left side looking upstream, and point *S2* is on the right side looking upstream.

When considering criteria (1), finding an obvious boundary between deltaic protrusion and the regional non-deltaic shoreline is not trivial, because deltaic deposition declines exponentially away from the source. In simple cases, such as wave-dominated cuspate deltas, the shoreline extents correspond to the maximum curvature of the delta shoreline protrusion as it transitions to the regional shoreline trend (Extended Data Figure 3c). In non-obvious cases, we aim to select the location that marks a transitional zone between deltaic and non-deltaic, and because of this, individual points may have different interpretations. In some more complicated cases, deltas can merge together at the shoreline and may share a point (Extended Data Figure 1c).

*Basinward extent point, towards open basin (OB)*

This point is defined by the location of deltaic land that is furthest basinward measured perpendicular to the deltaic shoreline vector (*LS*) (Extended Data Figure 2).

*Additional Considerations*

Channels that are both active and inactive in the imagery (i.e., holding water or not) were used for determining any of the above point locations that may be distinguished by the location of a channel body (i.e., *DN*, *S1*, *S2*) (Extended Data Figure 1a, channel on right demarcated by light blue arrow). We include inactive channels because they are evidence of deltaic deposition and there is no way to conclude if they are only temporarily inactive at the time the image was captured. Examples of inactive channels include temporarily inactive channels, such as ephemeral rivers or tidal channels, as well as channels that have been abandoned through avulsion but are still distinguishable in aerial imagery. For example, a delta's node may be chosen by an avulsion point of the parent channel creating a network of both currently active and inactive distributary channels downstream (e.g., Extended Data Figure 1a).

Additionally, obviously human-made channels/canals were not included when defining the lateral extent of a channel network. But, natural channels are often artificially stabilized by human activities, and we use these channels to define the delta extent when they could be clearly traced upstream to a natural channel (Extended Data Figure 1b).

Multiple rivers can interact to form one delta (e.g., one clear continuous protrusion from the shoreline). These multiple-source deltas are represented by one entry in the dataset (Extended Data Figure 1c, blue arrow indicates second river forming ID: 4023 on right). If two rivers create two deltas that are next to each other with some distributary overlap, they are represented by two entries in the dataset (Extended Data Figure Fig. 1c). Transitional cases are common, and thus the distinction between these two cases is not always clear. When possible, the existence or absence of separate shoreline protrusions were used to determine if multiple proximal rivers are creating one large delta or several slightly-overlapping deltas. If two or more rivers overlap via small tidal channels or human-made canals, they are not considered to be 'interacting' and are marked as separate entries in the dataset.

## 3. Calculating delta geomorphic area and habitable area

We calculate two area values: the geomorphic and habitable. We first remove land that falls within the delta extent polygon that is much higher elevation than the surrounding deltaic plain. High topography may be included inside a delta polygon when deltaic deposition fills in areas between pre-existing high topography. For example, this occurred in the Acheloos delta (Greece)[44]. To objectively remove high elevation non-deltaic areas for both the geomorphic and habitable area, we define elevation outliers as those points that are more than two times the inner quartile range of the elevation data for a given delta. Based on inspection, this effectively removes high elevation non-deltaic areas that are included in our delta polygon. Along the boundaries of the polygon we included the pixels if more than 50% of the pixel area was inside the polygon. Once clearly non-deltaic land is removed, we calculate the geomorphic area as the cumulative sum of all remaining pixels within the polygon. This area can include channels, shallow marine zones, and other bodies of water that are included in the polygon (Extended Data Figure 3).

Habitable area corresponds to the amount of land—geomorphic area minus the cumulative water (both fresh and saline) area—within each delta polygon. We call this habitable area under the assumption that people would not find water environments suitable for habitation, and only rarely live permanently on the water, although in some delta sectors people living on stilt habitations above the water. The land and water proportion for each pixel is determined at a subpixel level from a water mask that defines locations of water bodies like channels, wetlands, lakes, and the ocean. For this proportion we used a publicly available raster dataset of land and water area per pixel[17]. Pixel size is 30 arc seconds, or 1 km at the equator. Total habitable area is then the sum of all these proportions that fall within the polygon.

Because some deltas are smaller than the 30 arc second pixel size, not all deltas in the database have a geomorphic or habitable area value. Because of this there were 522 deltas that were given a value of NaN.

## 4. Delta Area Sensitivity and Validation

Our methodology draws a hard boundary separating deltaic from non-deltaic land. Population centers may straddle this boundary or lie just outside of it. A softer approach that also counts the population near the delta polygons may yield different estimates. To assess the sensitivity of our results to our choices of deltaic extent points, we create new polygons that are twice as large as the original by isotropically dilating the shape. This way we can also capture the population immediately adjacent to deltas. When we use these dilated polygons, we calculate a new global deltaic habitable area and population of 1,060,000 km$^2$ and 522 million. The population increases, as expected, but the population density stays relatively constant (492 ppl/km$^2$ instead of 478 ppl/km$^2$). This suggest to us that we are not missing any major population centers adjacent to our deltaic polygons. Note that even though we doubled the deltaic polygon, habitable area did not double (increased from 710,179 km$^2$ to 1,060,000 km$^2$) because it is always smaller than the polygon area because it does not include water bodies.

To validate our delta area methodology, we compare our area measurements based on the five points to deltaic areas reported by other authors. Even though we find it difficult to assess how other authors measured delta area, this allows us to understand if our measurement captures the spirit of what other workers tried to do. We cross-referenced our area data with that from Syvitski and Saito[38] and found that our delta area definition is remarkably close to theirs (Extended data Figure 4). In fact, the best fit linear regression nearly has a slope of 1:1 representing minimal bias, and the $R^2$ is 0.91. However, some of the measurements are significantly different than ours. In most cases this occurs because we use active and inactive channels to define the delta node and shoreline extents. If we just use active channels (those with water in recent imagery), then our areas for three deltas (Brazos, Niger, and Yukon) are revised downward and come much closer to previously published values (Extended Data Figure 4 and Extended Data Table 2). The only measurement that is still significantly different is that for the Amazon delta. We report an area of 85,667 km$^2$ and Syvitski and Saito[38] report an area of 471,000 km$^2$. Recent work by Brondizio et al.[45] suggests that the difference may be because the larger area includes the full extent of tidal channel activity not directly connected to the main river and channel network. In Brondizio et al.[45], the Amazon delta area was defined as a social-ecological system based on the intersection of physical and political administrative and demographic units, and this led to an estimated area of 160,662 km$^2$. Given the large uncertainty in the area of the Amazon delta, we show it on Extended Data Figure 4, but do not include it in the linear regression. The average percent error between our measurements and Syvitski and Saito (excluding the Amazon) is 50% and if we use the revised areas for the three deltas the average percent error is 36% (Extended Data Table 2).

## 5. Calculating deltaic population and designating country development categories.

We use the Oak Ridge National Laboratory LandScan dataset for all population calculations presented in the main text. We choose LandScan because it is based on census data, and uses a multivariable dasymetric model and imagery analysis, including nightlights, to spatially disaggregate the population. This is critical because it more accurately reflects the population at the coastline. Additionally, LandScan extends all coastal boundaries several kilometers seaward to capture the people living along the shoreline. The population for each deltaic area polygon was calculated by summing all the pixels of the population raster that fell within the delta extent polygon. Like the area calculations, pixels on the border were included if more than 50% of the area was inside the extent boundary. Because some deltas are smaller than the 30 arc-second pixel size, not all deltas in the database have a population value. There were 522 deltas that were given a value of NaN for population. These were excluded from the analysis.

We also compared our LandScan-derived population numbers to Global Population of the World (GPWv4)[17] and GRUMPv1 (ref [17]). Using the GPWv4 dataset, we calculate a total global deltaic population of in 2020 of 360 million people. GRUMPv1 is only available for year 2000 and we calculated a total population of 269 million, which is similar to 252 million calculated for LandScan for that year. The picture is similar if we consider the population within the 100-year floodplain for these different datasets. Using GRUMPv1 (year 2000) and GPWv4 (year 2020) we calculate that 37.8, 42.8 million people, respectively, reside in the 100-year floodplain.

Using a country boundary map as overlay, each delta was associated with a country, which in turn was designated to an economic development category based on the 2019 United Nations World Economic Situation and Prospects. Three categories are used: developed, developing, and least-developed countries. In addition, for the purpose of regional comparisons, we used country designation to assign each delta one of four global regions (Asia-Pacific, Americas, Europe-Central Asia, and Africa), as defined by the United Nations, as shown in Extended Data Figure 5.

### 6. Calculating 100-yr floodplain area and storm surge elevation

The 100-year floodplain area is calculated as the area at or below the elevation of the 100-year storm surge that is also connected to the ocean, either directly or via a river channel. Pixels are considered connected if any of the eight surrounding pixels have an elevation below the storm surge value. The elevation of the 100 year storm surge for each delta is determined by using the median value of all storm surge values calculated by Muis et al.[10] that fall within the deltaic polygon. This analysis does not account for the presence of coastal flood defenses. For instance, the Rhine delta has a high population within the 100-year floodplain, but their vulnerability is lower than less developed deltas. We use the Muis et al.[10] study of Global Tide and Storm Surge Reanalysis (GTSR) to estimate 100-year storm surge elevation because it is based on hydrodynamic modeling and has been rigorously validated by comparing modeled and observed sea levels. For instance, the DINAS-COAST Extreme Sea Levels (DCESL) dataset. DCESL overestimates extremes by 0.6 m whereas GTSR underestimates level by -0.2 m [46].

### 7. Calculating deltaic elevation

For all calculations involving elevation we use the Global Multi-resolution Terrain Elevation data from 2010 courtesy of the USGS. This composite dataset consists of elevation data from multiple sources. Because the data come from multiple sources the native resolution is not consistent and the raster has to be aggregated to a consistent resolution. We use an aggregate raster that reports the mean elevation of the native data at a resolution of 30-arc-second.

In a recent, publication, Muis et al.[46] pointed out that the datum for GTSR is mean sea level and that is not the same for the elevation data used here (EGM96). We opt to not correct the datum for GTSR so that we can make a direct comparison with Muis et al.[10].

# References


1. Knutson, T. R. *et al.* Tropical cyclones and climate change. *Nature geoscience* **3**, 157 (2010).
2. Nerem, R. S. *et al.* Climate-change–driven accelerated sea-level rise detected in the altimeter era. *Proceedings of the National Academy of Sciences* **115**, 2022-2025 (2018).
3. Woodruff, J. D., Irish, J. L. & Camargo, S. J. Coastal flooding by tropical cyclones and sea-level rise. *Nature* **504**, 44 (2013).
4. Syvitski, J. P. M. *et al.* Sinking deltas due to human activities. *Nature Geosci* **2**, 681-686 (2009).
5. Tessler, Z. *et al.* Profiling risk and sustainability in coastal deltas of the world. *Science* **349**, 638-643 (2015).
6. Ericson, J. P., Vorosmarty, C. J., Dingman, S. L., Ward, L. G. & Meybeck, M. Effective sea-level rise and deltas: Causes of change and human dimension implications. *Global and Planetary Change* **50**, 63-82 (2006).
7. Bianchi, T. S. *Deltas and humans: A long relationship now threatened by global change*. (Oxford University Press, 2016).
8. Le, T. V. H., Nguyen, H. N., Wolanski, E., Tran, T. C. & Haruyama, S. The combined impact on the flooding in Vietnam's Mekong River delta of local man-made structures, sea level rise, and dams upstream in the river catchment. *Estuarine, Coastal and Shelf Science* **71**, 110-116 (2007).
9. Caldwell, R. L. *et al.* A global delta dataset and the environmental variables that predict delta formation on marine coastlines. *Earth Surf. Dynam.* **7**, 773-787, doi:10.5194/esurf-7-773-2019 (2019).
10. Muis, S., Verlaan, M., Winsemius, H. C., Aerts, J. C. & Ward, P. J. A global reanalysis of storm surges and extreme sea levels. *Nature communications* **7**, 11969 (2016).
11. IPCC. Special Report on the Ocean and Cryosphere in a Changing Climate (SROCC) (2019).
12. Day Jr, J. W., Gunn, J. D., Folan, W. J., Yáñez-Arancibia, A. & Horton, B. P. Emergence of complex societies after sea level stabilized. *Eos, Transactions American Geophysical Union* **88**, 169 (2007).
13. Stanley, D. J. & Warne, A. G. Holocene sea-level change and early human utilization of deltas. *GSA Today* (1997).
14. Kennett, D. J. & Kennett, J. P. Early state formation in southern Mesopotamia: Sea levels, shorelines, and climate change. *Journal of Island & Coastal Archaeology* **1**, 67-99 (2006).
15. Small, C. & Nicholls, R. J. A global analysis of human settlement in coastal zones. *Journal of coastal research*, 584-599 (2003).
16. McGranahan, G., Balk, D. & Anderson, B. The rising tide: assessing the risks of climate change and human settlements in low elevation coastal zones. *Environment and urbanization* **19**, 17-37 (2007).
17. Center for International Earth Science Information Network - CIESIN - Columbia University. (NASA Socioeconomic Data and Applications Center (SEDAC), Palisades, NY, 2018).
18. Twilley, R. R. *et al.* Co-evolution of wetland landscapes, flooding, and human settlement in the Mississippi River Delta Plain. *Sustainability Science*, 1-21, doi:10.1007/s11625-016-0374-4 (2016).
19. Higgins, S., Overeem, I., Tanaka, A. & Syvitski, J. P. Land subsidence at aquaculture facilities in the Yellow River delta, China. *Geophysical Research Letters* **40**, 3898-3902 (2013).
20. Syvitski, J., Vorosmarty, C. J., Kettner, A. J. & Green, P. Impact of humans on the flux of terrestrial sediment to the global coastal ocean. *Science* **308**, 376-380 (2005).
21. Higgins, S. A. Advances in delta-subsidence research using satellite methods. *Hydrogeology Journal* **24**, 587-600 (2016).
22. Anthony, E. J. *et al.* Linking rapid erosion of the Mekong River delta to human activities. *Scientific reports* **5**, 14745 (2015).

23 Stanley, D. J. Nile Delta: extreme case of sediment entrapment on a delta plain and consequent coastal land loss. *Marine Geology* **129**, 189-195 (1996).

24 Tessler, Z. D., Vörösmarty, C. J., Overeem, I. & Syvitski, J. P. A model of water and sediment balance as determinants of relative sea level rise in contemporary and future deltas. *Geomorphology* **305**, 209-220 (2018).

25 Szabo, S. *et al.* Population dynamics in the context of environmental vulnerability: comparison of the Mekong, Ganges-Brahmaputra and Amazon delta regions. (2016).

26 Nagendra, H., Bai, X., Brondizio, E. S. & Lwasa, S. The urban south and the predicament of global sustainability. *Nature Sustainability* **1**, 341 (2018).

27 Eakin, H. C., Lemos, M. C. & Nelson, D. R. Differentiating capacities as a means to sustainable climate change adaptation. *Global Environmental Change* **27**, 1-8 (2014).

28 Mansur, A. V., Brondizio, E. S., Roy, S., Soares, P. P. d. M. A. & Newton, A. Adapting to urban challenges in the Amazon: flood risk and infrastructure deficiencies in Belém, Brazil. *Regional environmental change* **18**, 1411-1426 (2018).

29 Vörösmarty, C. J. *et al.* Battling to save the world's river deltas. *Bulletin of the Atomic Scientists* **65**, 31-43 (2009).

30 Giosan, L., Syvitski, J., Constantinescu, S. & Day, J. Climate change: protect the world's deltas. *Nature News* **516**, 31 (2014).

31 Edmonds, D. A., Paola, C., Hoyal, D. C. J. D. & Sheets, B. A. Quantitative metrics that describe river deltas and their channel networks. *Journal of Geophysical Research* **116**, F04022 (2011).

32 Serafin, K. A., Ruggiero, P., Parker, K. & Hill, D. F. What's streamflow got to do with it? A probabilistic simulation of the competing oceanographic and fluvial processes driving extreme along-river water levels. *Nat. Hazards Earth Syst. Sci.* **19**, 1415-1431, doi:10.5194/nhess-19-1415-2019 (2019).

33 Zscheischler, J. *et al.* Future climate risk from compound events. *Nature Climate Change* **8**, 469 (2018).

34 Kulp, S. A. & Strauss, B. H. New elevation data triple estimates of global vulnerability to sea-level rise and coastal flooding. *Nature Communications* **10**, 4844, doi:10.1038/s41467-019-12808-z (2019).

35 Vousdoukas, M. I. *et al.* Climatic and socioeconomic controls of future coastal flood risk in Europe. *Nature Climate Change* **8**, 776 (2018).

36 Milliman, J. D. & Farnsworth, K. L. *River discharge to the coastal ocean: a global synthesis*. (Cambridge University Press, 2011).

37 Paola, C. *et al.* Natural Processes in Delta Restoration: Application to the Mississippi Delta. *Annu. Rev. Mar. Sci* **3**, 3.1-3.25 (2011).

38 Syvitski, J. & Saito, Y. Morphodynamics of deltas under the influence of humans. *Global and Planetary Change* **57**, 261-282 (2007).

39 Orton, G. J. & Reading, H. G. Variability of deltaic processes in terms of sediment supply, with particular emphasis on grain size. *Sedimentology* **40**, 475-512 (1993).

40 Wright, L. D. & Coleman, J. M. Variation in morphology of major river deltas as functions of ocean wave and river discharge regimes. *The American Association of Petroleum Geologists Bulletin* **57**, 370-398 (1973).

41 Smart, J. S. & Moruzzi, V. L. Quantitative properties of delta channel networks. *Zeitschrift fur Geomorphologie* **16**, 283-300 (1972).

42 Morisawa, M. in *Models in Geomorphology* Vol. Allen and Unwin (ed M.J. Woldenberg) 239-268 (St Leonards, NSW, Australia, 1985).

43 Pizzuto, J. E. Sediment diffusion during overbank flows. *Sedimentology* **34**, 301-317 (1987).

44 Anthony, E. J. Wave influence in the construction, shaping and destruction of river deltas: A review. *Marine Geology* **361**, 53-78 (2015).
45 Brondizio, E. S. *et al.* A conceptual framework for analyzing deltas as coupled social–ecological systems: an example from the Amazon River Delta. *Sustainability Science* **11**, 591-609 (2016).
46 Muis, S. *et al.* A comparison of two global datasets of extreme sea levels and resulting flood exposure. *Earth's Future* **5**, 379-392 (2017).

## Supplementary Information containing data from this paper is available in the online version of the paper

## Acknowledgements

This research was supported by National Science Foundation award EAR 1812019, 1426997, 1135427, and support from the Prepared for Environmental Change initiative at Indiana University, both awarded to D.A.E.

## Author Contributions

D.A.E., R.L.C., and E.B. conceived of the study. D.A.E. executed the study and wrote the initial draft. R.L.C. performed the deltaic area mapping and assisted with data analysis. E.B. and S.S performed the socioeconomic data analysis. All authors discussed the results and contributed to writing the manuscript.

## Author Information

Reprints and permissions information are available at www.nature.com/reprints. The authors have no competing financial interests. Correspondence and requests for materials should be addressed to D.A.E. (edmondsd@indiana.edu). All data and material used in this paper will be made publicly available through scholarworks.iu.edu upon publication.

**Extended Data Table 1: Global delta dataset sorted by various parameters.** All sorting is by largest and show the top ten for each. Population density only shows the seven deltas with more than 150,000 people and greater than 10,000 people/km$^2$. For population density we only sort through those deltas with more than 150,000 people to avoid including densely populated that do not have many people living on them.

| ID | River Name | Country | Geomorphic Area (km2) | Habitable Area (km2) | Population year 2000 | Population year 2010 | Population year 2017 | Population density year 2017 (ppl/km$^2$) | Population in 100-year floodplain year 2017 |
|---|---|---|---|---|---|---|---|---|---|
| ***Sorted by Population 2017*** | | | | | | | | | |
| 4027 | Ganges | Bangladesh | 80174.17 | 68849.46 | 77233952 | 103549568 | 105461968 | 1532 | 2329660 |
| 0001 | Nile | Egypt | 28344.80 | 26359.72 | 32425994 | 38046124 | 45221260 | 1716 | 3120992 |
| 1537 | Yangtze | China | 16993.03 | 13321.07 | 21098204 | 23900496 | 31375546 | 2355 | 1635680 |
| 4158 | Mekong | Vietnam | 39465.66 | 37595.35 | 15867872 | 17418370 | 17924756 | 477 | 1962159 |
| 0124 | Niger | Nigeria | 34553.93 | 32517.17 | 9617618 | 11071605 | 12662285 | 389 | 39278 |
| 1449 | Pearl | China | 5613.34 | 5150.60 | 5754290 | 9504483 | 12065796 | 2343 | 4505003 |
| 4204 | Red | Vietnam | 8254.05 | 7394.86 | 9892108 | 10212460 | 10623076 | 1437 | 4273955 |
| 1538 | Guanhe | China | 19735.02 | 19216.04 | 11551084 | 11751276 | 10541032 | 549 | 8531302 |
| 4050 | Irawaddy | Myanmar | 28671.67 | 25629.22 | 7281147 | 9841221 | 9715010 | 379 | 13378 |
| 4137 | Chao Pharya | Thailand | 4090.40 | 3941.90 | 5041581 | 6063585 | 8061067 | 2045 | 11784 |
| ***Sorted by Population density 2017*** | | | | | | | | | |
| 2671 | Neva | Russia | 41.89 | 31.16 | 233369 | 370745 | 531676 | 17062 | 0 |
| 0083 | St. Paul | Liberia | 20.40 | 11.18 | 8212 | 92230 | 184532 | 16506 | 6 |
| 1772 | Arakawa | Japan | 52.26 | 49.59 | 850973 | 693158 | 753413 | 15194 | 0 |
| 1771 | Edo | Japan | 20.22 | 17.89 | 143140 | 182428 | 220347 | 12319 | 135 |
| 1841 | Yodo | Japan | 74.77 | 57.88 | 839601 | 677576 | 690775 | 11935 | 0 |
| 1514 | Minjiang | China | 85.50 | 67.16 | 258610 | 353819 | 684109 | 10187 | 0 |
| 1855 | Ota | Japan | 34.71 | 29.39 | 383684 | 323803 | 294351 | 10016 | 0 |
| ***Sorted by population in 100 year floodplain*** | | | | | | | | | |
| 1538 | Guanhe | China | 19735.02 | 19216.04 | 11551084 | 11751276 | 10541032 | 549 | 8531302 |
| 1449 | Pearl | China | 5613.34 | 5150.60 | 5754290 | 9504483 | 12065796 | 2343 | 4505003 |
| 4204 | Red | Vietnam | 8254.05 | 7394.86 | 9892108 | 10212460 | 10623076 | 1437 | 4273955 |
| 0001 | Nile | Egypt | 28344.80 | 26359.72 | 32425994 | 38046124 | 45221260 | 1716 | 3120992 |
| 4027 | Ganges | Bangladesh | 80174.17 | 68849.46 | 77233952 | 103549568 | 105461968 | 1532 | 2329660 |
| 4158 | Mekong | Vietnam | 39465.66 | 37595.35 | 15867872 | 17418370 | 17924756 | 477 | 1962159 |
| 2700 | Rhine | Netherlands | 3341.13 | 2740.86 | 1950636 | 2098707 | 2075289 | 757 | 1869518 |
| 1537 | Yangtze | China | 16993.03 | 13321.07 | 21098204 | 23900496 | 31375546 | 2355 | 1635680 |
| 1450 | Dong | China | 725.47 | 639.34 | 836432 | 2609015 | 3229268 | 5051 | 1003818 |
| 1991 | Agano | Japan | 338.55 | 324.48 | 639318 | 585962 | 577002 | 1778 | 250278 |
| ***Sorted by geomorphic area*** | | | | | | | | | |
| 3672 | Amazon | Brazil | 84429.42 | 58747.72 | 375797 | 646335 | 746287 | 13 | 5208 |
| 4027 | Ganges | Bangladesh | 80174.17 | 68849.46 | 77233952 | 103549568 | 105461968 | 1532 | 2329660 |

| | | | | | | | | | | |
|---|---|---|---|---|---|---|---|---|---|---|
| 3419 | Mississippi | USA | 51124.89 | 39829.07 | 2851512 | 2887614 | 3065114 | 77 | 27438 |
| 4158 | Mekong | Vietnam | 39465.66 | 37595.35 | 15867872 | 17418370 | 17924756 | 477 | 1962159 |
| 0124 | Niger | Nigeria | 34553.93 | 32517.17 | 9617618 | 11071605 | 12662285 | 389 | 39278 |
| 0001 | Nile | Egypt | 28671.67 | 25629.22 | 7281147 | 9841221 | 9715010 | 379 | 13378 |
| 4050 | Irawaddy | Myanmar | 28344.80 | 26359.72 | 32425994 | 38046124 | 45221260 | 1716 | 3120992 |
| 3672 | Amazon | Brazil | 22522.62 | 20698.41 | 69834 | 105932 | 160743 | 8 | 47 |
| 3691 | Orinoco | Venezuela | 21059.68 | 14590.52 | 55 | 130 | 187 | 0 | 0 |
| 1538 | Guanhe | China | 19735.02 | 19216.04 | 11551084 | 11751276 | 10541032 | 549 | 8531302 |

**Extended Data Table 2: Comparison between geomorphic area measurements (this study) and Syvitski and Saito[38].** Revised area shows deltaic area that only includes the active channel network.

| River | ID | Geomorphic Area ($km^2$) | Revised Area ($km^2$) | Syvitski and Saito (2007) area ($km^2$) | % difference with geomorphic area |
|---|---|---|---|---|---|
| Nile | 1 | 28344 | | 24,512 | 15.63 |
| Niger | 124 | 34533 | 18910 | 17,135 | 101.53 |
| Colorado (California) | 1122 | 394 | | 634 | 37.85 |
| Pearl | 1449 | 5613 | | 5200 | 7.94 |
| Yangtze | 1537 | 16993 | | 35,000 | 51.45 |
| Huanghe | 1560 | 6084 | | 5710 | 6.55 |
| Kolyma | 2357 | 4108 | | 6400 | 35.81 |
| Indigirka | 2363 | 7115 | | 4800 | 48.23 |
| Yana | 2372 | 4188 | | 1200 | 249.00 |
| Lena | 2380 | 21059 | | 24,000 | 12.25 |
| Pechora | 2629 | 1869 | | 3000 | 37.70 |
| Vistula | 2684 | 1234 | | 500 | 146.80 |
| Ebro | 2867 | 229 | | 338 | 32.25 |
| Rhone | 2876 | 1382 | | 1540 | 10.26 |
| Po | 2952 | 655 | | 1050 | 37.62 |
| Danube | 3017 | 3700 | | 4200 | 11.90 |
| MacKenzie | 3148 | 12363 | | 13,000 | 4.90 |
| Yukon | 3228 | 18295 | 5620 | 5200 | 251.83 |
| Mississippi | 3419 | 51124 | | 38,568 | 32.56 |
| Brazos | 3428 | 756 | 77 | 60 | 1160.00 |
| Colorado | 3431 | 83 | | 38 | 118.42 |
| Parana | 3593 | 3,850 | | 3,617 | 6.44 |
| Orinoco | 3691 | 22636 | | 35,642 | 36.49 |
| Amazon | 3696 | 85667 | | 467,000 | 81.66 |
| Magdalena | 3713 | 1969 | | 7500 | 73.75 |
| Tigris–Euphrates | 3805 | 2027 | | 3850 | 47.35 |
| Indus | 3842 | 12763 | | 6780 | 88.24 |
| Krishna | 4010 | 1458 | | 2100 | 30.57 |
| Godavari | 4011 | 4791 | | 4400 | 8.89 |
| Mahanadi | 4022 | 6608 | | 5900 | 12.00 |
| Ganges/Brahma | 4027 | 80174 | | 105,641 | 24.11 |
| Irrawaddy | 4050 | 28671 | | 30,570 | 6.21 |
| Chao Pharya | 4137 | 4090 | | 5500 | 25.64 |
| Mekong | 4158 | 39465 | | 49,000 | 19.46 |
| Red River | 4204 | 8254 | | 11,400 | 27.60 |
| Fly | 4981 | 3402 | | 2800 | 21.50 |

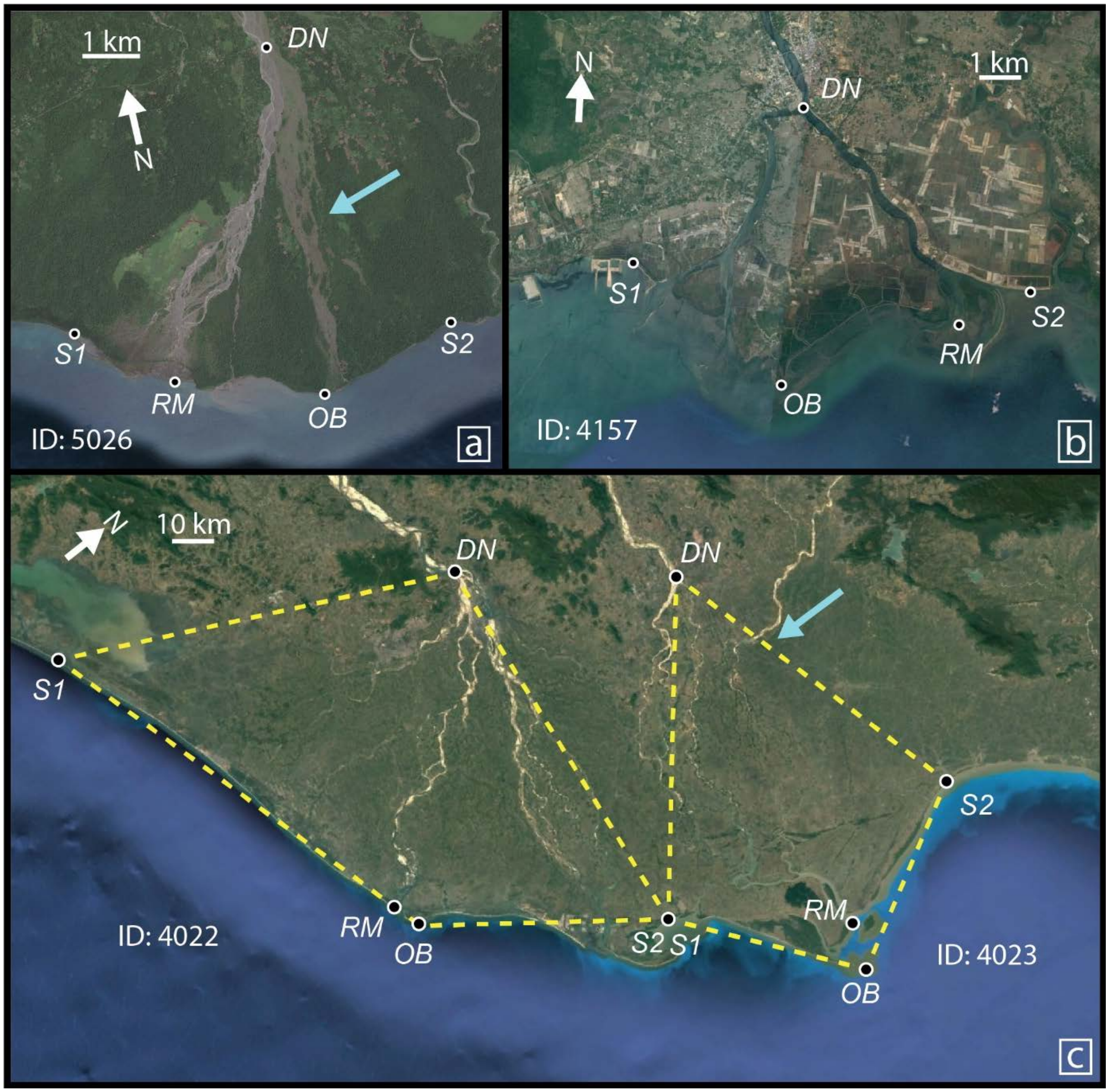


**Extended Data Figure 1: Examples of the five points that define the delta polygon.** (a) Example where *DN* location is chosen using relict channel (marked with blue arrow). (b) Example of human influenced delta. (c) Example of two deltas with separate IDs that share a lateral shoreline point. Delta on the right shows an example where two rivers, the one marked *DN* and one with the blue arrow, combine to form a single delta (ID: 4023). Dashed yellow lines show the delta polygons used in this study

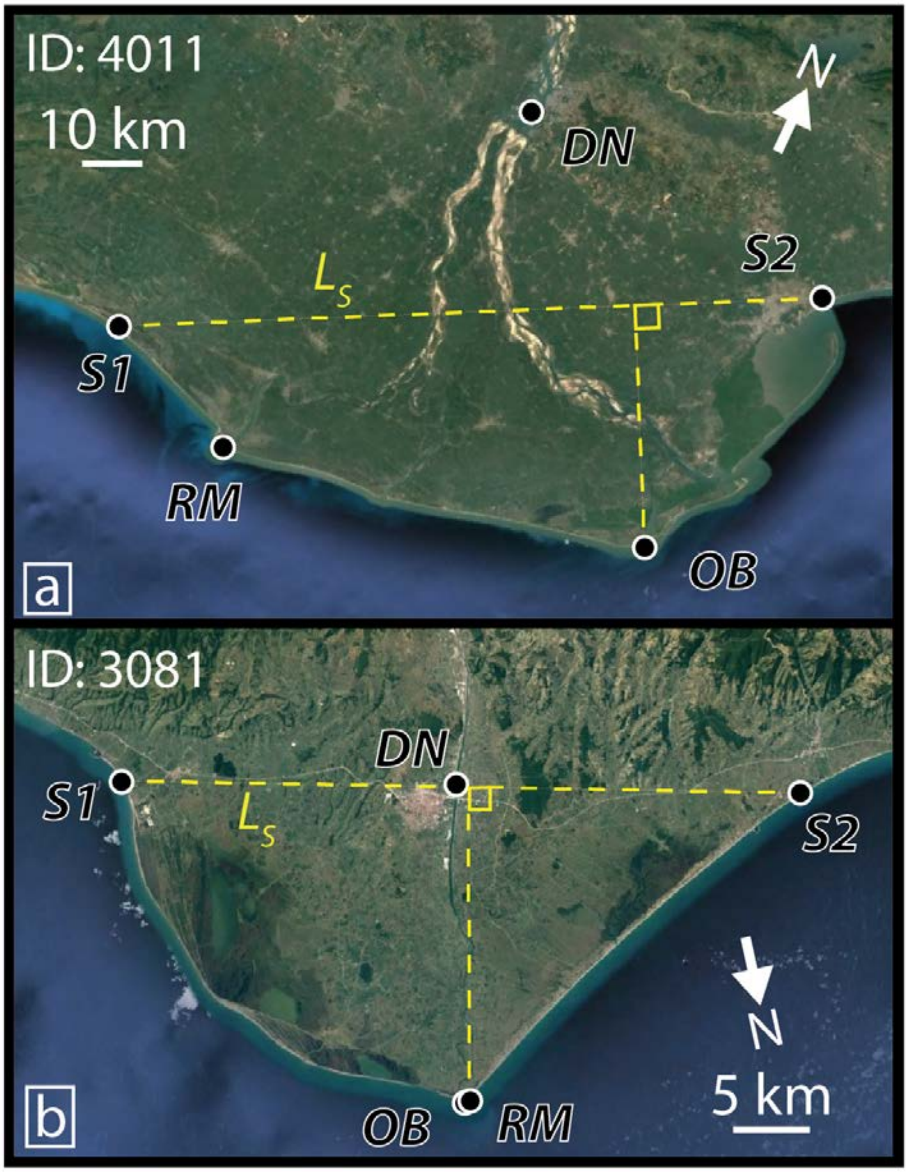


**Extended Data Figure 2: Examples showing how *DN* and *OB* are determined.** A local shoreline vector ($L_s$) is determined between points *S1* and *S2*. The delta node (*DN*) is given as either (a) the upstream most bifurcation of the parent channel the most upstream point or (b) the intersection of the main channel and $L_s$. If both criteria are present, then the point that is farthest upstream is selected.

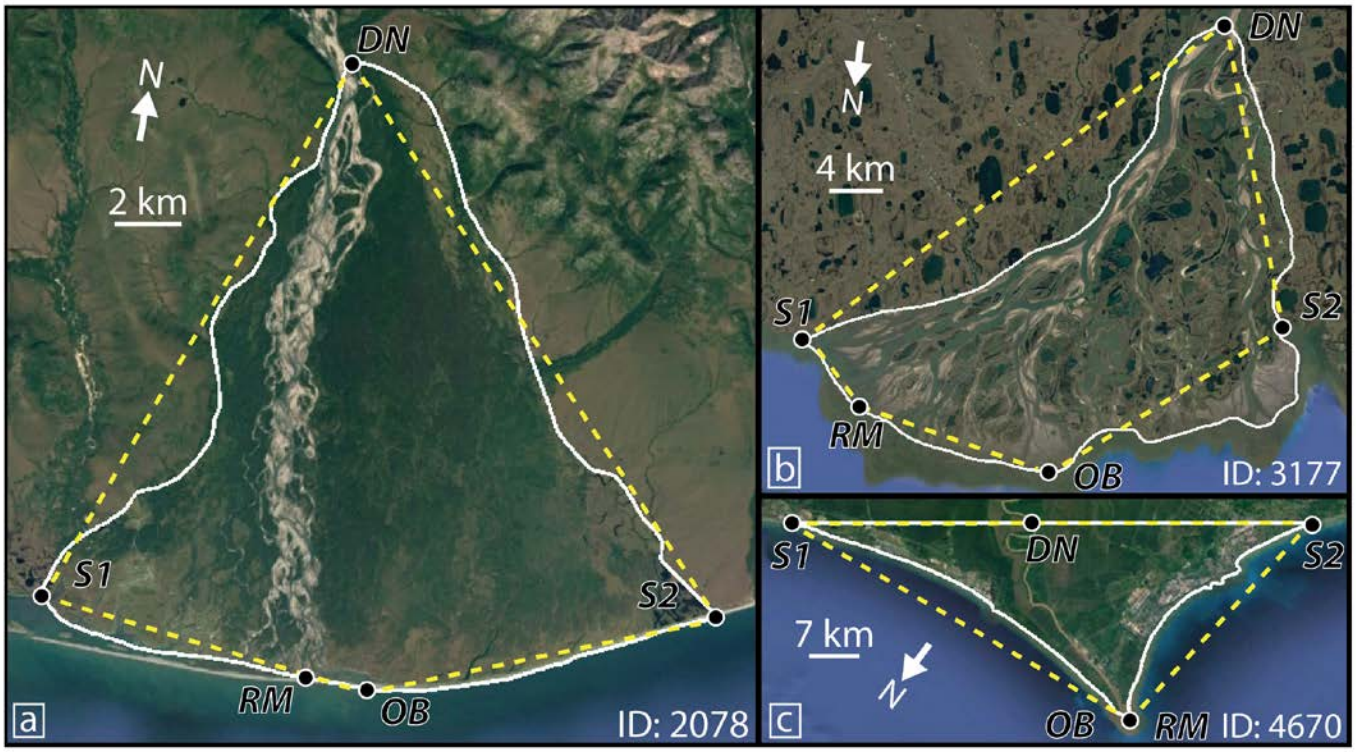


**Extended Data Figure 3: Examples of delta polygons.** Dashed yellow lines show the delta polygons used in this study, and white traced line is the boundary of the delta estimated by the contact between putative delta sediment and non-deltaic. (a,b,c) All three deltas show that the yellow polygon captures the first order shape of the delta.

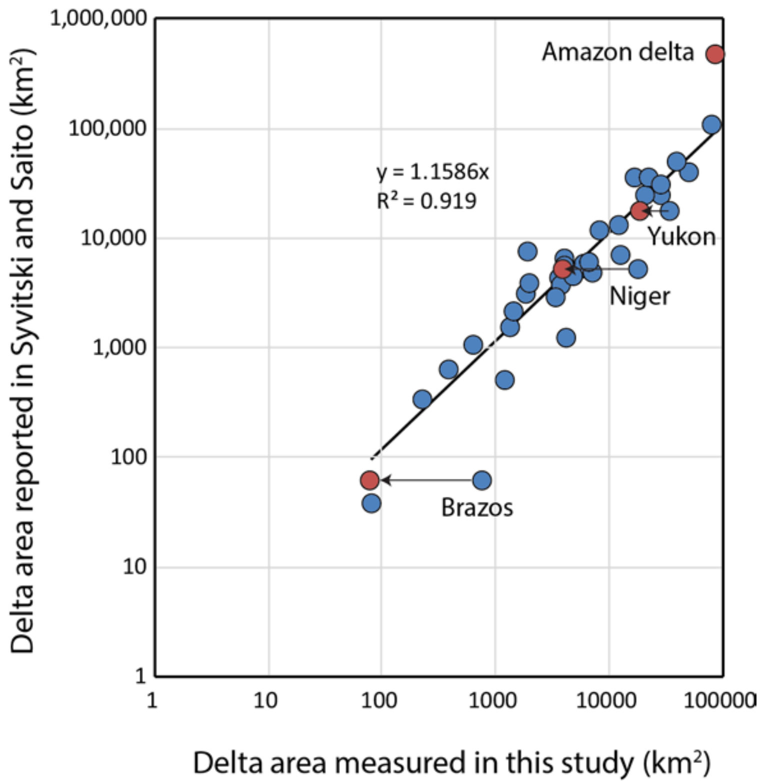


**Extended Data Figure 4: Comparison of geomorphic delta area measured in this study against Syvitski and Saito[17].** Best fit line is shown using the revised areas (shown in red) of Brazos, Niger, and Yukon deltas (see text for details). If the original geomorphic areas are used the relationship becomes $y=1.095x$, $R^2=0.87$. In both best fit calculations we do not include the Amazon delta since the area reported in Syvitski and Saito[17] is one-half an order of magnitude different than ours.

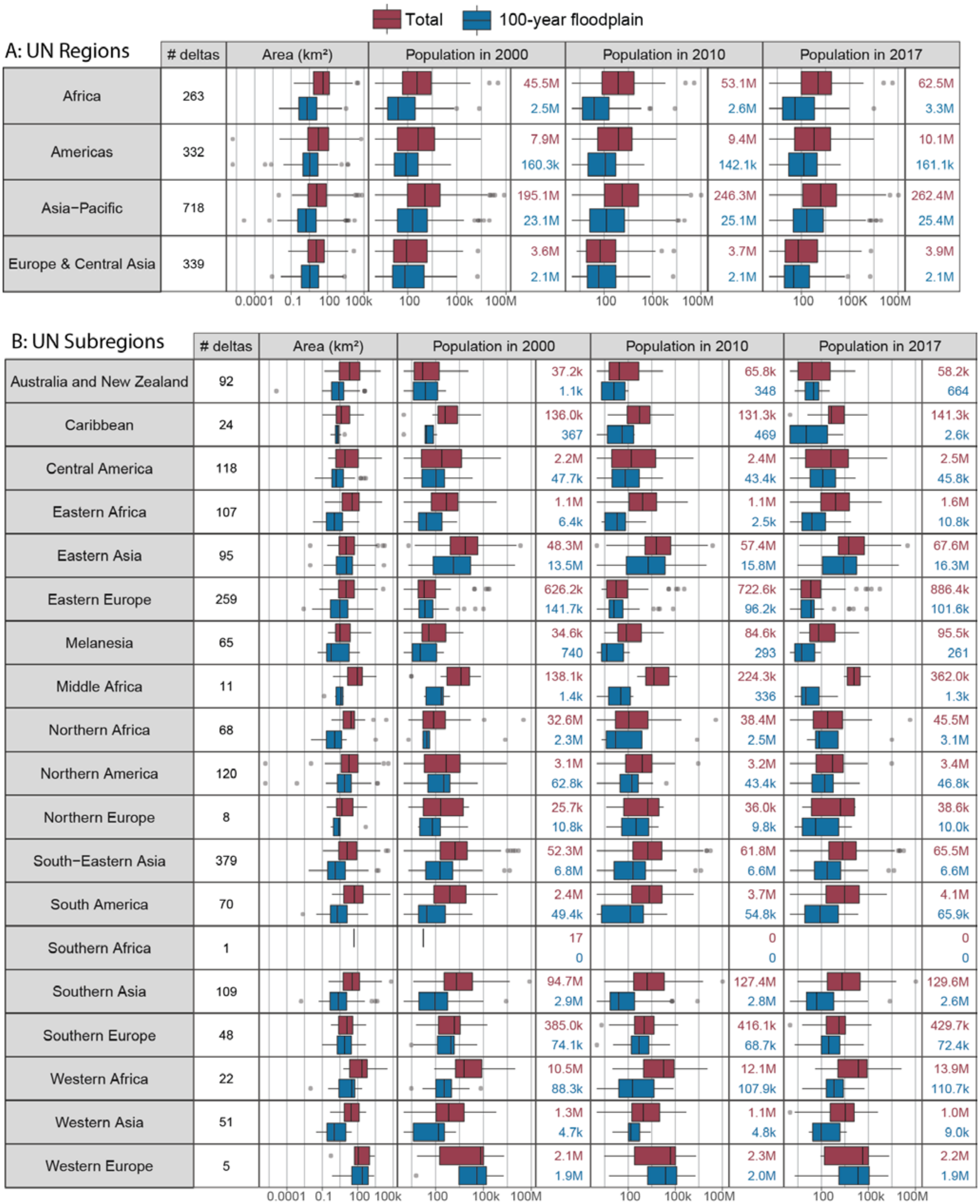


**Extended Data Figure 5: Deltaic area and population broken up by United Nations regions and subregions.**